9620 *Biochemistry* **2010,** *49,* 9620–9629
DOI: 10.1021/bi101237w

BIOCHEMISTRY
including biophysical chemistry & molecular biology
Article

Redox Linked Conformational Changes in Cytochrome c_3 from *Desulfovibrio desulfuricans* ATCC 27774[†,‡]

Vitor B. Paixão, Hans Vis, and David L. Turner*

Instituto de Tecnologia Química e Biológica, Universidade Nova de Lisboa, Rua da Quinta Grande 6, 2780-156 Oeiras, Portugal

Received August 3, 2010; Revised Manuscript Received September 20, 2010

ABSTRACT: Cytochrome c_3 from *Desulfovibrio desulfuricans* ATCC 27774 appears to be capable of receiving two protons and two electrons from hydrogenase for transport to the membrane, and converting electronic energy into proton motive force. Detailed studies of the mechanism require control both of the redox state and of the protonation state of the protein; hence, structure determination of the protein in solution by NMR is the preferred method. This work compares the structures of the protonated protein in the fully oxidized and fully reduced states as a first step toward elucidating the pH-dependent and redox-state-dependent conformational changes that drive the energy transduction. These high-resolution structures revealed significant localized differences upon change of redox state, even though the global folds of the two families of structures are similar. There are concerted redox-linked motions within the protein that bring E61 and K75 closer to heme II in the oxidized form. This is consistent with an electrostatically driven movement that may provide an important contribution to the previously measured positive cooperativity between hemes I and II. No significant conformational changes were observed that might be related to redox−Bohr effects; the families of structures represent mainly protonated forms, and therefore, pH dependence should not play a major role in the observed structural rearrangements.

Cytochromes c_3 isolated from *Desulfovibrio* spp. are periplasmic proteins which play a central role in energy transduction by coupling the transfer of electrons and protons from hydrogenase. By receiving both electrons and protons that result from the conversion of H_2, the redox−Bohr effect in cytochromes c_3 allows part of the free energy of the conversion to be used to release protons in the more acidic environment of the periplasm (*1*, *2*).

Because of their small size (ca. 13−14 kDa) and proximity of the hemes, cytochromes c_3 display homo- and heterocooperative effects arising from redox interactions between neighboring hemes (redox−redox interactions) and redox−Bohr interactions between hemes and protonatable centers (*3*−*7*) which allow them to work as small energy transduction devices (*8*, *9*). These interactions are responsible for the fine modulation of the redox potentials of the heme groups so that each cytochrome can be functionally optimized.

Despite their structural homology, the thermodynamic characterization of these proteins revealed that their redox and redox−Bohr interactions show significant variations (*2*, *5*, *9*−*13*). Indeed, reduction potentials ranging from −352 to −62 mV, redox interactions from 59 to −52 mV, and redox−Bohr interactions from −88 to −4 mV were determined for several cytochromes c_3 (*11*, *14*).

The oxidized and reduced solution structures for cytochromes c_3 from *D. vulgaris* and *D. gigas* have been determined and used to probe the structural basis for the network of functional cooperativities in these cytochromes (*15*−*18*).

Of all the cytochromes c_3 characterized so far, the one isolated from *Desulfovibrio desulfuricans* ATCC 27774 ($Dd27c_3$[1] hereafter) is distinctive since the pH dependence of its redox potentials involves two separate pK_a values (*11*, *12*) in contrast with the other cytochromes c_3 studied so far which have just one. Crystal structures of $Dd27c_3$ have been determined by X-ray diffraction (*19*, *20*), and the microscopic thermodynamic properties are well established (*11*). The first heme to oxidize is heme I followed by hemes II, IV, and III. No positive redox cooperativity is found between hemes, in contrast with *D.gigas* and *D. vulgaris*, but positive cooperativity is observed between the acid−base centers and the hemes, as expected from electrostatics. However, 21 thermodynamic parameters are needed to characterize the four redox centers and two protonatable groups in *D. desulfuricans* together with their pairwise interactions. Some of these could not be defined with the available data and were set to zero, namely, the proton−proton interaction, the interaction of the first acid−base center with heme I, and the interactions between the second acid−base center and hemes II, III, and IV (*11*).

Deviations from simple electrostatic interactions occur as a result of conformational changes that alter the distance between charges or modify the local dielectric constant. The oxidized protein should be deprotonated at pH 7.6, used for the crystal structures, and the reduced protein would be in a mixed protonation state. However, it is necessary to map the conformational

[†]This work was supported by the research grants PTDC/QUI/65640/2006 and REDE/1517/RMN/2005; V.B.P. was supported by the fellowship BD/5830/2001, all from Fundação para a Ciência e a Tecnologia (Portugal).

[‡]The structure data and the chemical shifts are deposited in the Protein Data Bank with accession numbers 16674 and 16443 and in the BioMagResBank with the accession numbers 2KSU and 2KMY for the reduced and oxidized structures, respectively.

*Corresponding author. Tel: 351 21 4469821. Fax: 351 21 4428766. E-mail: turner@itqb.unl.pt.

[1]Abbreviations: $Dd27c_3$, *Desulfovibrio desulfuricans* ATCC 27774.

 Published on Web 10/01/2010

changes that accompany reduction and protonation separately in order to understand the functional significance of the interactions. To that end, the solution structures of fully oxidized and reduced forms of *Dd27c*$_3$ were determined in this work. In each case, the pH of the sample was set below that of the groups involved in the redox−Bohr interactions (pH 4.2 and pH 6.4 respectively) to ensure that any conformational change depended primarily on the redox state.

MATERIALS AND METHODS

Sample Preparation. Cytochrome *c*$_3$ was purified from *D. desulfuricans* ATCC 27774 as described in the literature (*14*, *21*). For NMR experiments in H_2O, the protein was lyophilized from H_2O and suspended in 92% H_2O/8% ^2H_2O to a final concentration of approximately 2 mM. The pH was adjusted to 6.4 in an anaerobic chamber (Mbraun MB 150 I) by the addition of 0.1 M NaO^{2}H or ^{2}HCl for ^2H_2O samples and 0.1 M NaOH or HCl for H_2O samples. The pH values measured are direct meter readings without correction for isotope effects (*22*). Complete reduction of the samples was achieved by the reaction with hydrogen gas in the presence of catalytic amounts of hydrogenase isolated from *Desulfovibrio gigas* and *Desulfovibrio vulgaris*. To prevent bacterial growth, an antibiotic cocktail (70 μm ampicillin, 50 μm kanamycin, and 50 μm chloramphenicol) was added to the sample in H_2O.

For the preparation of the oxidized sample, the protein was dissolved in 90% H_2O/10% ^2H_2O and in 100% ^2H_2O to a final concentration of 1.8−2 mM. The pH was adjusted to 4.2 for the structure determination (uncorrected pH reading).

NMR Spectroscopy. *Reduced State Spectra*. ^{1}H NMR spectra were obtained on a Bruker DRX-500 spectrometer equipped with a 5 mm inverse detection probe head with an internal B_0 gradient coil and on a Bruker AV-800 equipped with a z-gradient cryoprobe.

Two-dimensional (2D) NMR spectra were acquired at 298 K. Acquisition was made in the phase sensitive mode by the States-TPPI method (*23*) collecting 4096 (t_2) × 1024 (t_1) data points to cover a sweep width of 10 kHz, with 64 scans per increment in 500 MHz spectra and 2048 (t_2) × 1024 (t_1) data points for a sweep width of 12 kHz with 64 scans per increment in the 800 MHz spectra. NOESY spectra were acquired with mixing times of 80 and 100 ms (*24*−*26*) with the SCUBA sequence (*24*) for the 500 MHz spectra and with the WATERGATE sequence (*27*) for water suppression in the 800 MHz spectra. Total correlation spectra were acquired using the clean TOCSY pulse sequence (*28*−*30*) with spin lock periods of 40 and 60 ms. COSY (*23*, *31*) and DQF-COSY (*32*, *33*) spectra were also recorded. Raw data were multiplied by a pure sine-squared function in both dimensions. 2D spectra were typically processed to a final size of 2k × 2k points. Polynomial baseline corrections were applied in both dimensions of each spectrum. Data were processed using XWINNMR and topspin software (Bruker, Rheinstetten). Proton chemical shifts are referenced to the resonances of the methyl groups in DSS at 0.0 ppm using water as the internal reference.

Oxidized state spectra. A series of 2D spectra were recorded on a Bruker DRX 500 spectrometer at 283, 298, 305, 310, and 315 K. NOESY spectra (*25*, *26*) were acquired at 298 K with 20 and 120 ms mixing times using standard pulse sequences with WATERGATE (*27*) and SCUBA (*24*) techniques. The short mixing time spectra were used for the analysis of heme and heme ligand resonances as well as for some protons very close to the hemes. TOCSY spectra were acquired with mixing times of 40 and 70 ms using the clean TOCSY sequence (*28*−*30*). COSY spectra were also recorded (*31*). The spectra were processed in a way similar to that used for the reduced state spectra.

Assignment and Integration. *Reduced State*. The software package XEASY (version 1.2; ETH, Zurich) (*34*) was used to display and annotate spectra. The assigned NOESY cross-peaks were integrated and converted into volume restraints with the program SPARKY (*35*). NOE volumes were measured in the 80 ms NOESY spectra at pH 6.4, cross-peaks involving protons separated by fixed distances, and all intraheme cross-peaks except those involving the propionate groups were excluded. Integration was performed by Gaussian and Lorentzian function fitting for isolated peaks and with sum data heights in a box or ellipse surrounding the peak for more overlapped peaks. The baseline around each individual peak was determined and used to correct the measured volume.

Oxidized State. The same software was used for spectral analysis of the oxidized spectra. Integration was performed with XEASY version 1.2; ETH, Zurich (*34*), either by manual integration for isolated peaks or with line-shape integration for overlapped peaks with baseline correction. Cross-peaks involving protons separated by fixed distances and all intraheme cross-peaks, except these involving the propionate groups and the thioether groups, were excluded from integration. Measured volumes were used to obtain an overall scaling factor relating the 120 ms mixing time NOESY spectra of samples in H_2O and ^2H_2O (*17*).

At later stages of the assignment procedure, pseudocontact shifts were obtained by subtraction of the chemical shifts in the reduced state from those of the same protons in the oxidized state and were used to calculate the magnetic susceptibility tensors. The predicted dipolar shifts were used as a guide for further assignment and in the elimination of misassignments, and helped to extend the assignment of the reduced form (*36*).

Determination of Restraints. *Reduced State*. The minimum uncertainty in any measured volume (δV) was estimated from the intensity of the smallest recognizable peaks in the H_2O spectrum and used as input for the program INDYANA (*37*). The program computes upper limit volumes (upv's) as $\langle V \rangle + \max(\delta V, \Delta V)$ and lower limit volumes (lov's) as $\langle V \rangle - \Delta V$, where $\langle V \rangle$ and ΔV are the average and difference of volumes for each pair of symmetrical cross-peaks, respectively. If one peak in a pair could not be measured, its volume is treated as zero. The inclusion of upv's and hence lower limit distance constraints makes automatic calibration of the NOEs possible and ensures that structures do not have protons in close proximity in the absence of experimental evidence. The conservative approach of applying a cutoff volume effectively limits these constraints to about 4 Å, which minimizes the risk of distorting structures through anomalously weak NOEs (*15*−*18*).

For degenerate or completely overlapped peaks, upper volume limits (lower distance constraints) were applied to both protons. At later stages of structure calculation, some of the potentially overlapping peaks could be specifically assigned as the various possibilities were eliminated by reference to the structure, therefore providing a lower volume limit also. For the degenerate H^{δ} and H^{ε} ring protons of fast-flipping residues, it is often possible to identify which side of the ring is involved because the pair of degenerate protons has a separation of 4.3 Å, which is large with respect to the distances that give rise to strong NOEs. In the preliminary stages of structure calculation, all cross-peaks from

degenerate ring protons are treated as nonspecific, with the exception of one chosen to distinguish the two sides of the ring. During structure refinement, individual NOEs were assigned specifically as in the case of nondegenerate protons, with the aid of the program GLOMSA (*38*).

Oxidized State. Because of paramagnetic relaxation, some cross-peaks that were visible in the 20 ms NOESY spectrum disappear at 120 ms; as a consequence, all cross-peaks involving heme groups and heme ligands were measured from the 20 ms H_2O spectrum.

In some cases, integrals were taken from the spectrum in which the cross-peak was more intense, and a separate calibration was used for the two mixing times, with a single additional parameter determining the ratio of scaling factors for each class of peaks. Instead of integrating every peak in both spectra, the cross-peak volumes at both mixing times were calculated with respect to preliminary structures to indicate which spectrum was appropriate for each cross-peak. Peaks with intensities predicted to increase by less than a factor of 2 between 20 and 120 ms were measured at both mixing times, and the largest volume was used in each case.

The two sets of integrals (20 and 120 ms) were processed separately to convert them into upper and lower volumes using the algorithm described previously and used in the program INDYANA (*37*). Before being used in the final structure calculations, these four sets of values (20 and 120 ms, upper and lower volumes) were corrected for reduction of the NOE intensities by electron−nuclear dipolar relaxation caused by the paramagnetic heme groups (*15*).

Additional Restraints. Three nonstandard residues were used for both structure calculations: fast-flipping aromatic residues with pseudoatoms to define the orientations of the planes (*17*, *39*, *40*), flexible heme groups, and proline residues with fixed upper limit distances for ring closure (*17*, *37*, *41*). In addition, for the oxidized state, two types of histidine axial ligands were defined to take into account the iron−nitrogen bond (*17*, *41*), the magnetic axes (*41*), and the torsion angle that defines the orientation of the histidine ring plane with respect to the heme plane (*37*). The torsion angles were not constrained but provide a convenient measure of ligand geometry. In the final stages of structure refinement, the calculated structures were checked for short (less than 2.5 Å) distances between assigned protons that should give rise to significant NOEs. Even if no peaks were visible at the predicted frequencies, the volume was measured and used in further calculations. In this way, a lower limit distance restraint defines a minimum distance between protons if there is no NOE in the spectra.

Correction of Volume Restraints for the Oxidized State. In paramagnetic proteins, the NOE intensities of protons near the heme groups are reduced due to relaxation caused by the dipolar coupling to the unpaired electrons on the iron atoms of the hemes. Correction for this paramagnetic leakage has been shown to increase the resolution of calculated structures in regions close to the paramagnetic center (*42*, *43*).

The contribution to longitudinal relaxation from the dipolar interaction between a nuclear spin and each unpaired electron is described by the following equation (*44*):

$$\rho_I^{\text{para}} = \frac{1}{10}\left(\frac{\mu_0}{4\pi}\right)^2 \frac{\gamma_I^2 g_e^2 \mu_B^2}{r^6}\left(\frac{3\tau_S}{1+\omega_I^2\tau_S{}^2} + \frac{\tau_S}{1+(\omega_I-\omega_S)^2\tau_S{}^2} + \frac{6\tau_S}{1+(\omega_I+\omega_S)^2\tau_S{}^2}\right)$$

where γ_I is the nuclear gyromagnetic ratio, r is the distance between the proton and the metal center, τ_S is the correlation time for electron spin relaxation, μ_B is the Bohr magneton, and ω_I and ω_S are the Larmor frequencies of the proton and the electron. Assuming that the unpaired electrons are localized on the iron atoms, the constants can be combined in a parameter k such that $\rho_i = kr^{-6}$. For simplicity, τ_S is assumed to be equal for the four heme groups. The value of k was estimated from the ratio of cross-peak intensities in the 20 and 120 ms spectra. By adding this electron−nucleus dipolar contribution to the diagonal elements of the internuclear dipole−dipole relaxation matrix calculation, the NOE intensity can be obtained (*45*, *46*). Cross-peak intensities were then calculated with and without paramagnetic effects using $k = 6 \times 10^5$ Å^6 s^{-1} for the paramagnetic relaxation and $\tau_R = 8$ ns for the diamagnetic terms, with averaged distances from a family of preliminary structures. A correction factor was obtained for each cross-peak from the ratio of the two calculated values, $I_{ij}^{\text{para}}/I_{ij}^{\text{dia}}$, and each upper and lower volume limit was divided by its correction factor (*42*, *43*). Using constraints obtained with different mixing times reduces the need for correction: the largest calculated volume ratios were less than 10. Since this approach is approximate, all distance restraints were softened by a percentage to allow a margin for error and for the effects of spin diffusion. For this purpose, the cross-peak intensities calculated with the inclusion of paramagnetic relaxation were replaced by scaled measured values and back-transformed to give theoretical distances. Those distances that were outside the range obtained from the maximum and minimum experimental volumes were used to calculate a ratio that was used to relax all distance restraints.

Dipolar Shifts As Restraints for the Oxidized State. Dipolar (pseudocontact) shifts are useful for structure determination and refinement for paramagnetic proteins (*36*) due to the dependence on the position of the nucleus relative to the paramagnetic centers and their magnetic axes. Simultaneous calculation of the structure and the magnetic susceptibility tensors to fit dipolar shifts is implemented in the program PARADYANA (*41*).

Approximate dipolar shifts were obtained by subtracting the shifts of the reduced protein from those observed in the oxidized protein. To ensure that the use of dipolar shifts would not undermine the detection of any change in structure between the oxidized and the reduced forms, some shifts were not considered in the calculation, namely, shifts of nonspecifically assigned diastereotopic pairs of protons (except when the values for both protons of the pair differ by less than 0.2 ppm), as well as shifts for H^N. Diamagnetic shifts were calculated for the family of structures in the reduced form and for a family of oxidized structures obtained without dipolar shifts and protons for which the difference in shifts from the two forms was greater than 0.2 ppm were excluded from the list of dipolar shifts. As a further test, the remaining dipolar shifts were used to fit the magnetic susceptibility tensor parameters to the coordinates of a preliminary set of 20 structures obtained without the use of dipolar shifts (*47*), with the uncertainty for the dipolar shifts set to ±0.2 ppm and the uncertainty for the atomic coordinates set to ±0.25 Å. Those dipolar shifts which were not accommodated by these uncertainties in more than 10 out of the 20 structures were rejected. Finally, if a side-chain proton was excluded, then so were the shifts of all protons further from the backbone.

Structure Calculations. The final reduced and oxidized structures were calculated with the program PARADYANA (*41*),

as in the case of *Desulfovibrio gigas* (*15*), *Desulfovibrio vulgaris* (*16*, *17*), and *Shewanella fridigimarina* (*48*). The program uses corrected NOE volumes, angle restraints, and dipolar shifts, as described above, and optimizes magnetic susceptibility tensors together with the parameters of the structure in the presence of paramagnetic centers.

A complete relaxation matrix analysis was used to estimate the error that might be induced by spin diffusion. Theoretical NOEs were replaced by scaled measured NOEs, and the combined NOE matrix was back-transformed to obtain interproton distances that take account of spin diffusion. The rmsd of the ratio between those calculated distances that deviated from the maximum or minimum distances obtained by automatic calibration in PARADYANA was used to loosen all of the distance restraints in subsequent structure calculations.

Structure Analysis. CHIMERA (version 1.24) (*49*) was used for visual interpretation with the preliminary structure calculations, as an aid to assignment, during structure refinement. The program MOLMOL (version 2.0) (*50*) was used for superimposition, visual inspection, calculation of mean structure, and of root-mean-square deviations from the mean structure. Stereochemical analysis of the structures was performed with the program WHAT IF (version 20030529-0952) (*51*). Identification and classification of the consensus secondary structure elements in the NMR structure ensemble, defined as those present in at least 50% of the structures, was accomplished with the program PROMOTIF (version 2.0) (*52*). Secondary structural shifts, which are dominated by the effect of heme ring currents, were calculated for the structures using the program TOTAL (*53*).

Diamagnetic Chemical Shift Calculations. Proton chemical shifts were calculated for the ensemble of the best NMR structures for both the oxidized and reduced states using the program TOTAL (*53*).

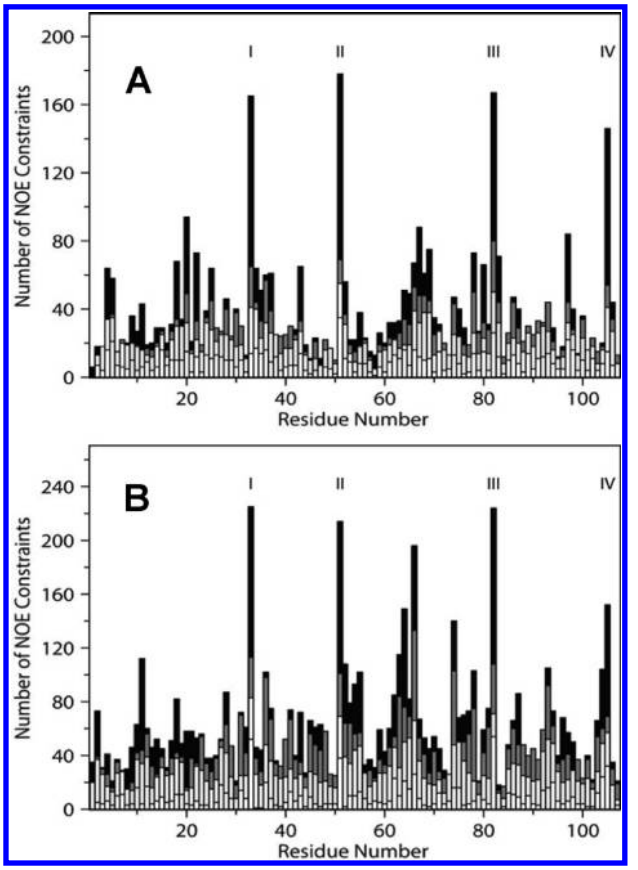

FIGURE 1: Number of NOE restraints per residue. Bars are white, light gray, dark gray, and black for intra residue, sequential, medium, and long-range restraints, respectively. Residues 33, 51, 82, and 105 also include restraints to hemes I, II, III, and IV, respectively. (A) Restraints for the structure of the reduced state. (B) Restraints for the oxidized state.

RESULTS

Structure Determination for the Reduced State. Assignment and Integration. Amino acid assignment was performed using the approach described by Wüthrich (*54*), assisted by predicted chemical shifts for the reduced protein, based on the preliminary structures of the oxidized form as well the X-ray structure of the reduced structure of *Dd27c*$_3$ (*19*). Spin systems were identified through analysis of the TOCSY and COSY spectra of ^2H_2O and H_2O solutions, and sequence-specific assignment was performed by analyzing NOESY spectra of the protein in H_2O and identifying sequential connectivities.

Sequential connectivities between H^N, H^α, and H^β protons are shown in Supporting Information Figure S1. All of the residues, with the exception of prolines (residues 2, 5, 8, 21, 24, 91, and 107), show at least one of the sequential connectivities between their H^N and H^N, H^α, or H^β of the preceding residue. For the proline residues, connectivities were obtained at least between the H^δ protons of the prolines and the H^α or H^β of the preceding residue. Two of the exchangeable hydroxyl group protons of Thr and Ser residues were also found (T98 and S63).

In total, 77% of all of the protons in this protein after excluding exchangeable protons other than backbone H^N were assigned. The chemical shifts have been deposited in the BioMagResBank database (http://www.bmrb.wisc.edu) under accession number BMRB-16674.

Calculation and Analysis of Structures. Assigned cross-peaks in the H_2O NOESY spectra were integrated and converted into volume restraints, resulting in 1107 lower limits (lov's) and 1339 upper limits (upv's). These were used as input for the program PARADYANA (*41*) together with a set of 133 fixed upper limit distances associated with ring closure in the flexible proline residues and heme groups, and the attachment of Histidine ligands (*17*, *37*, *41*).

The preliminary calculated structures were analyzed using the program GLOMSA (*55*) modified to take NOE volumes as input, and 26 stereospecific assignments were made for diastereotopic pairs of protons or methyl groups. The conversion of experimental data to distance constraints has an intrinsic uncertainty due to the spin diffusion effect, which was simulated by complete relaxation matrix calculations based on the initial protein structures, with τ_R = 8 ns. Calculated spin diffusion effects have errors that arise from the uncertainties in the atomic coordinates. Hence, we adopt a statistical approach in which all constraints are loosened far enough to eliminate the majority of distortions. Accordingly, a parameter was set in the program PARADYANA to loosen all distance restraints by 4%. An average of 23 NOE restraints per amino acid residue (10 lov's and 13 upv's) and 122 per heme residue (55 lov's and 67 upv's) were used for the final calculation (Figure 1). A total of 500 random conformers were used as starting points for annealing by the PARADYANA program. The 20 structures with the lowest target function values (from 2.40 Å^2 to 2.80 Å^2; average value 2.66 Å^2; range 17% from the lowest value) were selected as being representative of the solution structure of the protein. The

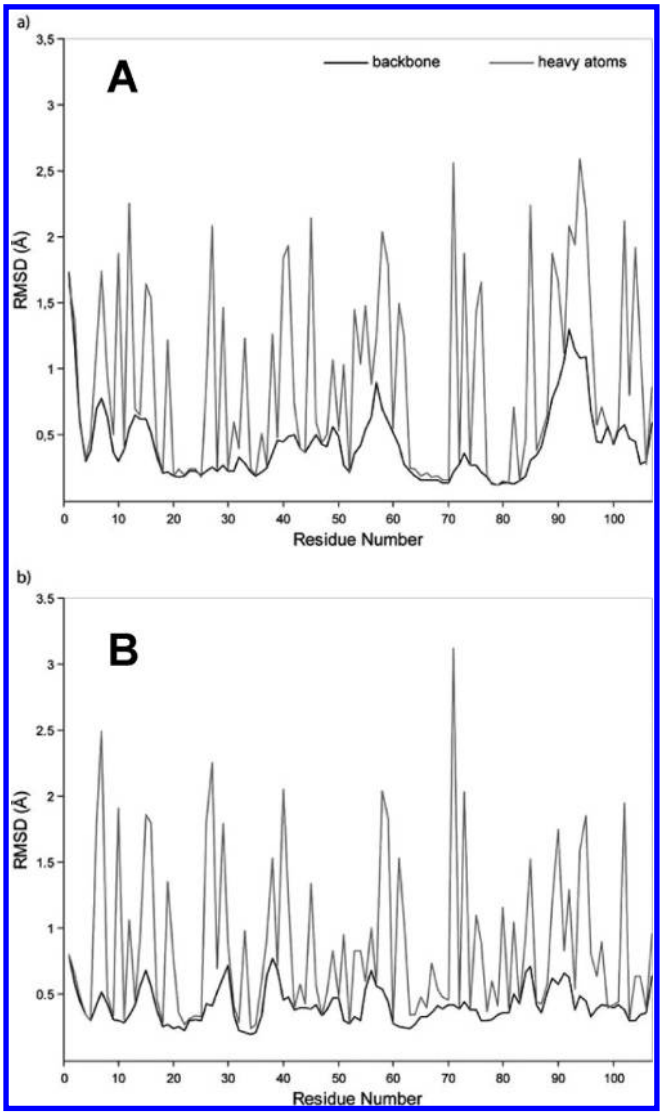

FIGURE 2: Average backbone and heavy atom rmsd values per residue with respect to the mean structure of the families of $Dd27c_3$ conformers. (A) Reduced form. (B) Oxidized form.

structures superimpose with an average backbone rmsd of 0.58 Å and a heavy atom rmsd of 1.28 Å with respect to the mean structure; the statistics for the family of structures are shown in Figure 2 and Table 2.

The Ramachandran plot (*56*) shows 59.5% of the residues in the most favored regions, 36.9% in the additionally allowed, 2.4% in the generously allowed, and 1.1% in the disallowed regions. Residues in the disallowed regions include K58 and K95, which show a low number of restraints per residue. A total of 108 hydrogen bonds were identified in the family of 20 structures with the program WHAT IF (using routine HBO), 25 of which were present in at least 50% of the structures. Chemical shifts were calculated for each proton in the NMR structures and compared with experimental values as described in Materials and Methods (Figure 4).

Structure Determination for the Oxidized State. Assignment and Integration. Assignments were obtained for the 107 residues and the four heme groups, using a combination of NOESY, TOCSY, and COSY experiments at different mixing times and temperatures. The axial histidine residues experience large paramagnetic shifts: the His ring protons were not observed, and the H^N, H^α, and H^β protons show large downfield shifts. Two of the exchangeable hydroxyl protons of Ser residues were found (S63 and 103). In total, 89% of the proton resonances after excluding exchangeable protons other than the backbone H^N atoms were assigned.

Table 1: Restraints Used for the Calculation of Reduced and Oxidized Cytochrome c_3 from *D. desulfuricans* ATCC 27774

distance restraints (reduced)	upper distance limits	lower distance limits
intraresidual	333	416
sequential ($\|1 - j\| = 1$)	275	350
medium range ($2 \leq \| i - j \| < 5$)	190	240
long range ($\|1 - j\| \geq 5$)	313	410
total	1111	1416

distance restraints (oxidized)	upper distance limits	lower distance limits
intraresidual	294	352
sequential ($\|1 - j\| = 1$)	502	624
medium range ($2 \leq \| i - j \| < 5$)	504	550
long range ($\|1 - j\| \geq 5$)	557	594
total	1857	2120

Restraints. A total of 1453 lower volume limits and 1774 upper volume limits were obtained from the NOESY spectra with a 120 ms mixing time. The spectra with a 20 ms mixing time yielded a further 191 lov's and 282 upv's. More restraints were obtained for the oxidized form than the reduced from, mainly because of the reduced spectral overlap in the presence of paramagnetic shifts. The detection of two hydroxyl protons in slow exchange with water in each of the forms suggests that the rigidity of the structure is unchanged. Stereospecific assignments were obtained using the program GLOMSA. Out of the 200 stereopairs with nondegenerate chemical shifts, 73 were stereospecifically assigned, and 55% of the restraints to fast-flipping aromatic residues were pseudostereospecifically assigned to one or the other side of the ring. A summary of the restraints used is presented in Table 1, and the number of restraints per residue is shown in Figure 1. Initial structures calculated with uncorrected NOE volumes were used as input for relaxation matrix calculations. Correction factors for paramagnetic leakage (*42*, *43*) were obtained as described in Materials and Methods. Structures calculated with these corrected restraints were used as input for relaxation matrix calculations to assess the influence of spin diffusion. The back-calculated distances exceeded the range of experimental restraints with an rmsd of 4% for the 20 ms data and 8% for the 120 ms data, and these values were used to soften all distance restraints in the final structure calculations.

Dipolar shifts contain important long-range structural information since they depend on the inverse cube of the distance from the metal centers as well as the orientation and anisotropy of the magnetic susceptibility tensors (*44*). Therefore, they can be used together with the other experimental restraints such as paramagnetic relaxation (*57*) and nuclear Overhauser enhancements (*58*), or even be used by themselves as restraints for structure refinement (*59*). Conversely, anomalous dipolar shifts may indicate misassignments; predictions of shifts from calculations and experimental temperature dependences were used as a guide for further assignment once preliminary structures were available (*36*). Experimental dipolar shifts were determined by subtracting the observed reduced protein shifts from the observed oxidized shifts. However, to allow for possible changes in the

diamagnetic contribution to the shifts of the oxidized and reduced forms due to structural differences, the shifts of some protons were excluded as described in Materials and Methods.

The NOE volume limits, together with dipolar shifts and the fixed upper limit distances were used as input for the program PARADYANA. With this program, the anisotropies of the magnetic susceptibility tensors as well as the orientation of their principal axes are optimized simultaneously with the annealing of each structure, such that the final family of structures reflects the uncertainty in all of the tensor parameters as well as the atomic coordinates.

Calculation and Analysis of Structures. Six hundred random conformers were used as starting points for annealing and the structures with the lowest target function values were selected as representative of the solution structure of the protein. The final family consists of 20 structures with 34% target function variation (ranging from 2.83 Å^2 to 3.82 Å^2, average value 3.48 Å^2) from the first to the last. The structures superimpose with an average backbone rmsd of 0.48 Å and a heavy atom rmsd of 1.18 Å with respect to the mean structure; the statistics for the family of structures are shown in Figure 2 and Table 2. For the oxidized structure, a total of 109 hydrogen bonds were identified in the family of 20 structures using the program WHAT IF (routine HBO), 30 of which were present in at least 50% of the structures. The Ramachandran plot for all of the relevant residues gave 71.4% residues in the most favored regions, 26.2% in the additionally allowed, and 2.4% in the generously allowed.

The average magnetic susceptibility tensors obtained for the family of structures are shown in Table 3. Besides providing a refinement of atomic coordinates through the dipolar shifts, the tensors can also be used to estimate the orientation of the axial ligands (*60*). In fact, for low-spin bis-histidinyl heme proteins it is predicted that the magnetic axes will rotate about the perpendicular to the heme in the opposite sense to the axial ligands. The data of Table 3 shows that the counter-rotation of the magnetic *y*-axis in the plane of the heme in the opposite sense to the axial ligand orientations holds for this protein as in several other cases of Dc_3 (*60*). This provides an independent test for the consistency of the chemical shifts used in this calculation as well as the proton structural coordinates and the geometry of the heme ligands. This internal consistency is further supported by the low value of the equatorial anisotropy for heme II that is associated with the large dihedral angle between the His ring planes. Yet another test is provided by comparing the geometry obtained by analyzing the paramagnetic shifts of the heme methyl groups (*61*).

Table 2: Summary of Scaling Factors, Restraint Violations, and Quality Analysis for the Final Families of Structures for Reduced and Oxidized Cytochrome c_3 from *D. desulfuricans*

parameter	reduced	oxidized
scaling factors		
proton−proton	29.89 ± 0.15	7.36 ± 0.03
proton−methyl	36.42 ± 0.10	8.78 ± 0.06
methyl−methyl	46.82 ± 0.28	11.79 ± 0.35
backbone proton−proton	28.64 ± 0.05	7.23 ± 0.03
Dyana target function		
average total (Å)	2.66 ± 0.12	3.43 ± 0.31
upper distance limit violations		
average maximum	0.28 ± 0.06	0.24 ± 0.06
number of consistent violatioxns (>0.2 Å)	0	0
lower distance limit violations		
average maximum	0.27 ± 0.04	0.29 ± 0.05
aumber of consistent violations (>0.2 Å)	0	1
Van de Waals violations		
average maximum	0.28 ± 0.01	0.26 ± 0.03
number of consistent violations (>0.2 Å)	0	1
dipolar shifts violations		
average maximum		0.48 ± 0.07
number of consistent violations (>0.2 Å)		1
Ramachandran plot (%)		
most favored	59.5	71.4
additionally allowed	36.9	26.2
generously allowed	2.4	2.4
disallowed	1.1	0
precision		
rmsd backbone (Å)	0.58 ± 0.10	0.48 ± 0.07
rmsd heavy atoms (Å)	1.28 ± 0.10	1.18 ± 0.08

DISCUSSION

Comparison between the Solution Structures of the Reduced and Oxidized States. Calculated diamagnetic shifts may be used to test the accuracy of the reduced structures: shifts were calculated for each unique nonexchangeable proton in the reduced NMR structures and compared with the experimental values (Figure 4A). These shifts are dominated by large ring current contributions from the hemes, and the good overall agreement is an assurance of the quality of the structures. Dipolar shifts were fitted as part of the structure determination for the oxidized protein (Figure 4B) and therefore do not provide a completely independent test. However, the quality of the fit and the relationship between the magnetic susceptibility tensors, the heme ligand orientations, and the Fermi contact shifts of the heme methyl groups demonstrate the quality of the structure (see Table 3). Also, despite the expectation that the magnetic susceptibility tensors of the hemes will have different temperature dependences, the simple measurement of the temperature dependence of chemical shifts provides a good estimate of the dipolar

Table 3: Properties of the Magnetic Susceptibility Tensors of the Four Hemes in *D. desulfuricans* Cytochrome c_3[a]

hemes	I	II	III	IV
$\Delta\chi_{ax} \times 10^{32}$ (m^3)	3.8 (0.2)	3.5 (0.1)	2.0 (0.1)	3.0 (0.4)
$\Delta\chi_{eq} \times 10^{32}$ (m^3)	−1.8 (0.1)	−0.8 (0.2)	−1.8 (0.2)	−2.4 (0.2)
in-plane rotation of χ_y (deg)	−52.5 (2.8)	−74.4 (8.8)	−158.5 (2.4)	−52.0 (4.1)
tilt angle of χ_z (deg)	3.9 (2.0)	5.0 (2.0)	7.0 (3.8)	5.2 (3.1)
average imidazole orientation ϕ (deg)	49.1 (2.9)	85.6 (3.6)	160.1 (5.6)	58.7 (4.4)
predicted orientation ϕ (deg)[b]	48.6	89.6	156.7	51.6
angle between imidazole planes β (deg)	5.5 (8.2)	73.0 (8.1)	21.8 (14.2)	29.1 (10.5)
predicted dihedral angle β (deg)[b]	11.3	60.6	25.3	8.9

[a]The in-plane rotation is given for the *y*-axis to allow direct comparison with the orientations of the imidazole planes as defined by ref *61*; note the opposite sign of the angle. [b]Predicted from chemical shifts using eq 5 of ref *61*.

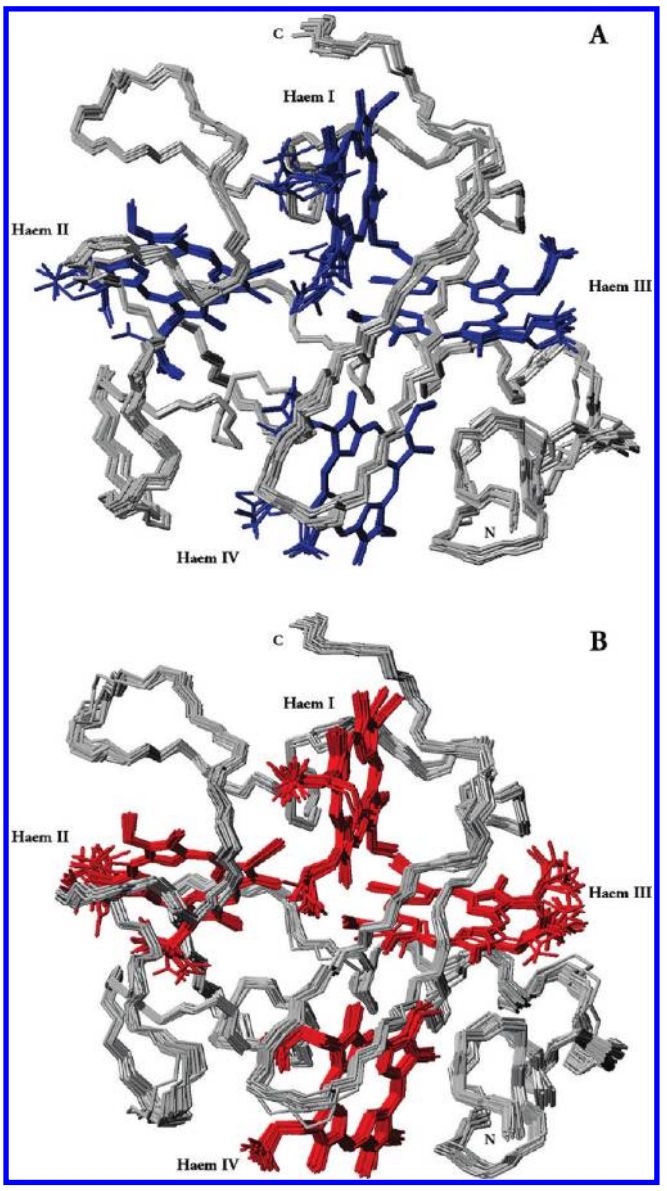

FIGURE 3: Backbone and hemes of the 20 lowest energy NMR structures of *D. desulfuricans* cytochrome c_3 for the (A) reduced state and (B) oxidized state. The peptide chain and the hemes are color-coded gray, blue (A), and red (B), respectively. The figure was produced using MOLMOL (*50*).

shifts of individual protons that correlates well with the observed values (Figure 4C).

The global rmsd of the superimposition of the mean structures of each family is 0.98 Å for backbone atoms and 1.34 Å for heavy atoms respectively, which is larger than might be expected on the basis of the uncertainty of the individual structures. The overall fold of the oxidized and reduced structures is very similar, with the position of the heme groups and Fe distances showing good agreement (Figure 3A and B), and only minor differences between the consensus secondary structure elements were identified. The two-stranded antiparallel β-sheet (V9-K12 and T17-F20) and one of the 3_{10}-helices (A23-H25) were found in both states of the structures. The α-helix (A81-S84) in the reduced form was found as a π-helix in the oxidized form, and the second 3_{10}-helix (V86-A88) in the reduced form was found as an α-helix in the oxidized state.

A few regions of the protein show differences between the reduced and oxidized form that are significantly larger than the

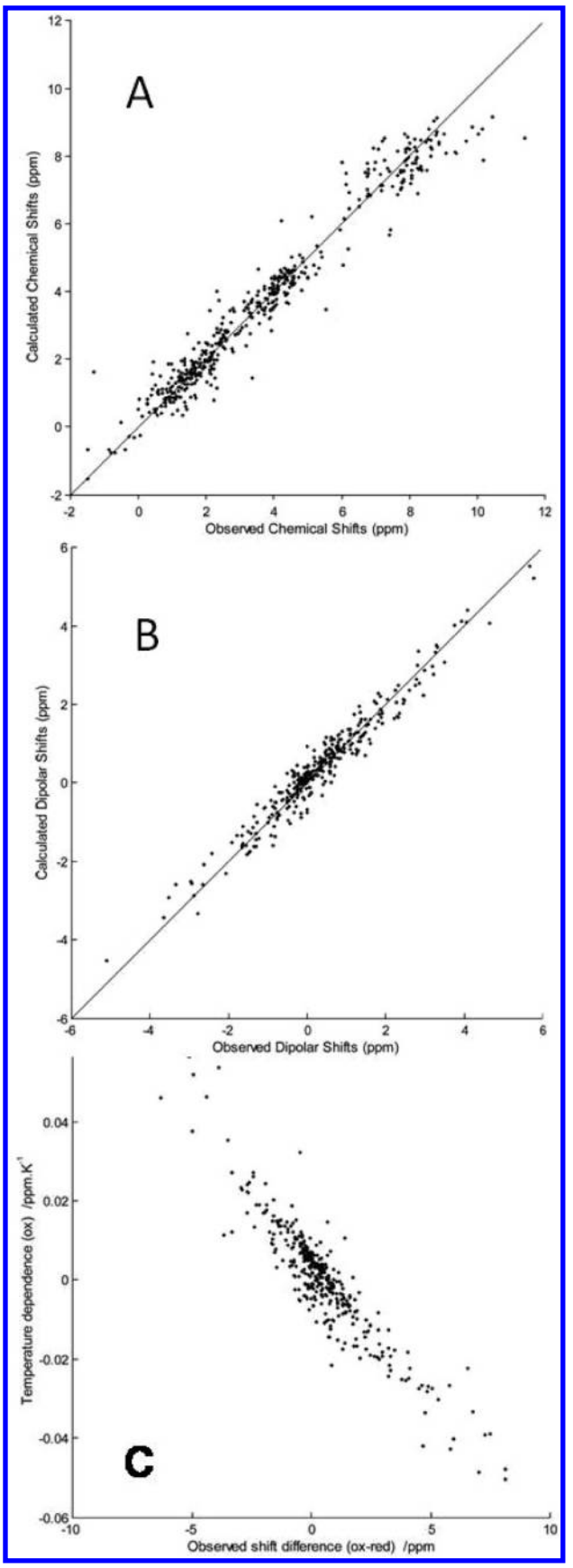

FIGURE 4: (A) Average calculated chemical shifts for protons in the 20 best *Dd27c*$_3$ NMR reduced structures versus observed chemical shifts. (B) Calculated dipolar shifts for the family of oxidized structures against the observed shifts. (C) Correlation of the measured temperature dependence of proton shifts on the oxidized protein against the observed dipolar shifts. Panels A and B include lines of unit slope.

global rmsd values, which may indicate redox-related structural changes (Figure 5). The largest differences are observed in the segments 11−20, 47−63, and 71−75. It is important to note that the heme core region is virtually unchanged between the two forms with only a few of the propionate groups showing some conformational disorder, usually related to higher solvent exposure. The segment comprising residues V11−F20 shows a slight but significant (with respect to the global rmsd) movement toward the propionates of heme IV upon reduction. All these residues are well-defined in the solution structure families with many NOEs involving the side chain atoms. The two small β strands identified in this zone are also conserved in both solution structures as well as in the X-ray structures of the reduced (1UP9) and oxidized (1UPD) forms (*19*). The backbone of the segment G47-S63 also moves, with L55, T56, and K59, closer to the propionates of heme IV in the oxidized cytochrome. This rearrangement brings E61 within hydrogen-bonding distance of propionate D of heme II (Figure 6). Earlier simulations identified E61 and propionate D of heme II as showing important contributions to the redox cooperativity of this cytochrome (*19*, *20*).

The X-ray structures of reduced and oxidized *Dd27c*$_3$ showed conformational changes involving residues K75, H76, and also propionate D of heme II as possible participants in the functional cooperativities of this protein. In solution, we also find a flexible region between R71 and K75 moving slightly closer to heme II upon oxidation, with K75 within H-bond distance of propionate D of heme II. The free histidine H76 has been identified as a likely redox−Bohr group (*19*), but it should be largely protonated in both forms studied here; it shows a high degree of conformational variability among the structures of each state, and therefore, the conformational changes are not significant.

Structural basis for the Redox and Redox−Bohr Couplings. Several cytochromes c_3 show positive redox cooperativity between hemes; the most positive effect in *Dd27c*$_3$ is between hemes I and II, which have a near-zero redox interaction despite their proximity, i.e., the electrostatic interaction is canceled by changes in conformation. As mentioned above, E61 shows a significant redox-linked conformational change with its charged carboxylate side chain moving closer to heme II upon oxidation, which is consistent with an electrostatically driven movement. A distinct cluster in the vicinity of heme II, comprising L74, K75, and the propionates of heme II, shows redox linked changes in conformation. A movement of L74 toward propionate A of heme II is observed with reduction, while K75 shifts closer to propionate D of the same heme upon oxidation. These changes may make an important contribution to the positive cooperativity observed for hemes I and II, which essentially titrate together. However, it is not possible to attribute the effect to isolated groups: it appears to involve concerted motions within the structure upon reduction (Figure 5).

The thermodynamic properties of *Dd27c*$_3$ reported in the literature have shown that the reduction potentials of the four hemes are pH dependent, the so-called redox−Bohr effect. This pH dependence in the range 5−9 is mediated by two distinct pK_a fitted with pK_a^{red} = 7.4 and 6.4 and pK_a^{ox} = 4.9 and 4.9 (the two are not distinguishable in the oxidized form) (*11*). Propionate D of heme I has been shown to play an important role in the functional cooperativities of cytochromes c_3 from several *Desulfovibrio* species (*11*, *15*−*17*, *62*), and from the structural, thermodynamic, and theoretical data it has also been suggested that the propionates of heme I play a similar role in *Dd27c*$_3$ (*19*). In particular, the acid−base center denoted H2 (*11*) shows a strong influence on the reduction potential of heme I. However, when comparing the oxidized and reduced structures in solution the propionates of heme I, which are relatively disordered, or its neighboring residues show no significant conformational modifications. In fact, both propionates are expected to be protonated at the chosen pH values (4.2 and 6.4, respectively).

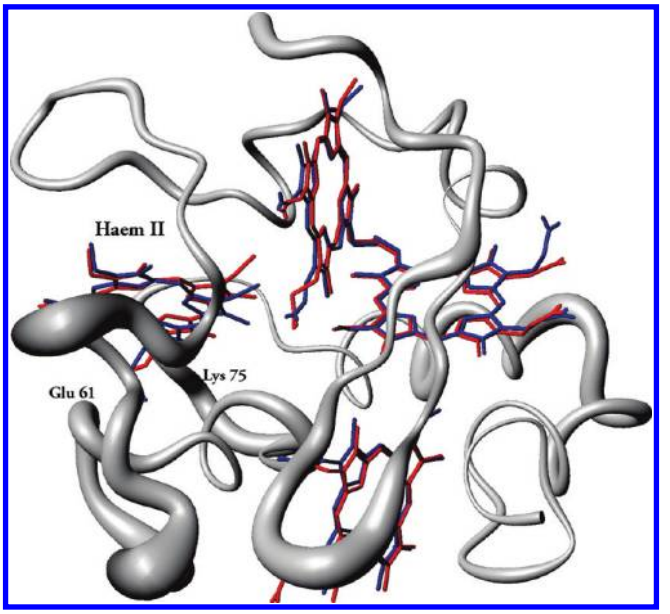

FIGURE 5: Redox state dependent conformational changes in cytochrome c_3 from *D. desulfuricans*. The diameter of the tube is proportional to the rms displacement between the mean oxidized structure and the mean reduced structure. The hemes of the reduced structure are colored blue, and those of the oxidized structure are red. The orientation is the same as that in Figure 3. The figure was produced using MOLMOL (*50*).

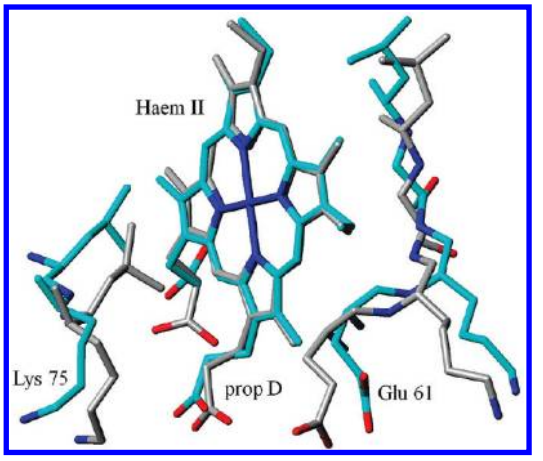

FIGURE 6: Conformations of heme II propionate D and residues Glu 61 and Lys 75 in the overall best NMR structures of reduced (cyan) and oxidized (gray) cytochrome c_3 from *D. desulfuricans*. Note that the orientations of the Lys N$^{\zeta}$ and Glu carboxylate are not well-defined. The figure was produced using MOLMOL (*50*).

Conclusions. High quality solution structures of reduced and oxidized cytochrome c_3 from *D. desulfuricans* ATCC27774 have been solved from NMR data obtained from samples at pH values chosen to ensure that both forms were in similar states of protonation with respect to the redox−Bohr protons.

The standard stereochemical checks as well as the good agreement with the experimental constraint data and between the calculated and experimental diamagnetic shifts is a good indication of the accuracy of the reduced structure. The structure

of the oxidized *Dd27c*$_3$ was calculated together with its magnetic properties: the magnetic susceptibility tensors obtained from the calculated family of structures provide an independent test for the structural geometry.

Comparison between the structures of tetraheme cytochrome c_3 in the reduced and oxidized states showed that the general backbone conformation is maintained as well as the orientation and position of the hemes. The segments involving residues 11−20, 47−63, and 71−75 show significant differences between the two forms, with a combined rearrangement of these regions leading to the movement of E61 toward a hydrogen-bond distance of propionate D of heme II, in agreement with the proposed contributions of E61 and heme II to the redox properties of *Dd27c*$_3$ (*19*, *20*). In fact the redox-linked movement of E61 and of a cluster involving K75 and the propionates of heme II may play an important role in the positive cooperativity observed between hemes I and II.

The reduction potentials of the four hemes of *Dd27c*$_3$ are pH dependent, and several previous studies link the propionates of heme I to an important role in the functional properties of this cytochrome. In solution, at the chosen pH values of the oxidized and the reduced samples (4.2 and 6.4 respectively), the ionizable centers involved in the redox−Bohr effect are essentially protonated in the structures obtained in this work, and no significant conformational changes are observed for heme I or neighboring residues when comparing the oxidized and reduced structures. The same situation occurs for the free histidine H76, which has been described as a likely redox−Bohr group (*19*): it is partly protonated in the reduced and oxidized forms and shows no significant conformational changes in solution.

In conclusion, comparing the reduced and oxidized structures in solution in the same protonation state allowed us to identify the redox related conformational changes that are important in the heme−heme cooperativity observed in this protein. This emerged as a concerted motion upon reduction involving several zones and is not attributable to isolated groups. Furthermore, the fact that the redox−Bohr effects are not observed could make this analysis more significant since the possible interference from pH dependent conformational changes is avoided.

ACKNOWLEDGMENT

This work was initiated and inspired by António Xavier (1943−2006).

SUPPORTING INFORMATION AVAILABLE

Sequential NOE connectivities for reduced and oxidized proteins. This material is available free of charge via the Internet at http://pubs.acs.org.

REFERENCES

1. Odom, J. M., and Peck, H. D. (1981) Hydrogen cycling as a general mechanism for energy coupling in the sulfate-reducing bacteria, *Desulfovibrio* sp. *FEMS Microbiol. Lett. 12*, 47–50.
2. Louro, R. O., Catarino, T., LeGall, J., and Xavier, A. V. (1997) Redox-Bohr effect in electron/proton energy transduction: cytochrome c3 coupled to hydrogenase works as a 'proton thruster' in *Desulfovibrio vulgaris*. *J. Biol. Inorg. Chem. 2*, 488–491.
3. Fan, K. J., Akutsu, H., Kyogoku, Y., and Niki, K. (1990) Estimation of microscopic redox potentials of a tetraheme protein, cytochrome c3 of *Desulfovibrio vulgaris*, Miyazaki F, and partial assignments of heme groups. *Biochemistry 29*, 2257–2263.
4. Turner, D. L., Salgueiro, C. A., Catarino, T., LeGall, J., and Xavier, A. V. (1994) Homotropic and heterotropic cooperativity in the tetraheme cytochrome c3 from *Desulfovibrio vulgaris*. *Biochim. Biophys. Acta 1187*, 232–235.
5. Turner, D. L., Salgueiro, C. A., Catarino, T., Legall, J., and Xavier, A. V. (1996) NMR studies of cooperativity in the tetraheme cytochrome c3 from *Desulfovibrio vulgaris*. *Eur. J. Biochem. 241*, 723–731.
6. Salgueiro, C. A., Turner, D. L., Gall, J. L., Xavier, A. V., and LeGall, J. (1997) Reevaluation of the redox and redox−Bohr cooperativity in tetraheme *Desulfovibrio vulgaris* (Miyazaki F) cytochrome c3. *J. Biol. Inorg. Chem. 2*, 343–349.
7. Park, J. S., Ohmura, T., Kano, K., Sagara, T., Niki, K., Kyogoku, Y., and Akutsu, H. (1996) Regulation of the redox order of four hemes by pH in cytochrome c3 from *D. vulgaris* Miyazaki F. *Biochim. Biophys. Acta 1293*, 45–54.
8. Louro, R. O., Catarino, T., Salgueiro, C. A., LeGall, J., and Xavier, A. V. (1996) Redox-Bohr effect in the tetraheme cytochrome c3 from *Desulfovibrio vulgaris*: a model for energy transduction mechanisms. *J. Biol. Inorg. Chem. 1*, 34–38.
9. Louro, R. O., Catarino, T., Turner, D. L., Picarra-Pereira, M. A., Pacheco, I., LeGall, J., and Xavier, A. V. (1998) Functional and mechanistic studies of cytochrome c3 from *Desulfovibrio gigas*: thermodynamics of a "proton thruster. *Biochemistry 37*, 15808–15815.
10. Paquete, C. M., Pereira, P. M., Catarino, T., Turner, D. L., Louro, R. O., and Xavier, A. V. (2007) Functional properties of type I and type II cytochromes c3 from *Desulfovibrio africanus*. *Biochim. Biophys. Acta 1767*, 178–188.
11. Paquete, C. M., Turner, D. L., Louro, R. O., Xavier, A. V., and Catarino, T. (2007) Thermodynamic and kinetic characterisation of individual hemes in multicentre cytochromes c3. *Biochim. Biophys. Acta 1767*, 1169–1179.
12. Louro, R. O., Catarino, T., LeGall, J., Turner, D. L., and Xavier, A. V. (2001) Cooperativity between electrons and protons in a monomeric cytochrome c(3): the importance of mechano-chemical coupling for energy transduction. *ChemBioChem 2*, 831–837.
13. Correia, I. J., Paquete, C. M., Louro, R. O., Catarino, T., Turner, D. L., and Xavier, A. V. (2002) Thermodynamic and kinetic characterization of triheme cytochrome c3 from *Desulfuromonas acetoxidans*. *Eur. J. Biochem. 269*, 5722–5730.
14. Coutinho, I. B., and Xavier, A. V. (1994) Tetraheme cytochromes. *Methods Enzymol. 243*, 119–140.
15. Brennan, L., Turner, D. L., Messias, A. C., Teodoro, M. L., LeGall, J., Santos, H., and Xavier, A. V. (2000) Structural basis for the network of functional cooperativities in cytochrome c(3) from *Desulfovibrio gigas*: solution structures of the oxidised and reduced states. *J. Mol. Biol. 298*, 61–82.
16. Messias, A. C., Aguiar, A. P., Brennan, L., Salgueiro, C. A., Saraiva, L. M., Xavier, A. V., and Turner, D. L. (2006) Solution structures of tetraheme ferricytochrome c3 from *Desulfovibrio vulgaris* (Hildenborough) and its K45Q mutant: the molecular basis of cooperativity. *Biochim. Biophys. Acta 1757*, 143–153.
17. Messias, A. C., Kastrau, D. H., Costa, H. S., LeGall, J., Turner, D. L., Santos, H., and Xavier, A. V. (1998) Solution structure of *Desulfovibrio vulgaris* (Hildenborough) ferrocytochrome c3: structural basis for functional cooperativity. *J. Mol. Biol. 281*, 719–739.
18. Harada, E., Fukuoka, Y., Ohmura, T., Fukunishi, A., Kawai, G., Fujiwara, T., and Akutsu, H. (2002) Redox-coupled conformational alternations in cytochrome c(3) from *D. vulgaris* Miyazaki F on the basis of its reduced solution structure. *J. Mol. Biol. 319*, 767–778.
19. Bento, I., Matias, P. M., Baptista, A. M., da Costa, P. N., van Dongen, W. M., Saraiva, L. M., Schneider, T. R., Soares, C. M., and Carrondo, M. A. (2004) Molecular basis for redox−Bohr and cooperative effects in cytochrome c3 from *Desulfovibrio desulfuricans* ATCC 27774: crystallographic and modeling studies of oxidized and reduced high-resolution structures at pH 7.6. *Proteins 54*, 135–152.
20. Louro, R. O., Bento, I., Matias, P. M., Catarino, T., Baptista, A. M., Soares, C. M., Carrondo, M. A., Turner, D. L., and Xavier, A. V. (2001) Conformational component in the coupled transfer of multiple electrons and protons in a monomeric tetraheme cytochrome. *J. Biol. Chem. 276*, 44044–44051.
21. Liu, M. C., Costa, C., Coutinho, I. B., Moura, J. J., Moura, I., Xavier, A. V., and LeGall, J. (1988) Cytochrome components of nitrate- and sulfate-respiring *Desulfovibrio desulfuricans* ATCC 27774. *J. Bacteriol. 170*, 5545–5551.
22. Glasoe, P. K., and Long, F. A. (1960) Use of glass electrodes to measure acidities in deuterium oxide. *J. Phys. Chem. 64*, 188–190.
23. Marion, D., and Wuthrich, K. (1983) Application of phase sensitive two-dimensional correlated spectroscopy (COSY) for measurements of 1H-1H spin-spin coupling constants in proteins. *Biochem. Biophys. Res. Commun. 113*, 967–974.

24. Brown, S. C., Weber, P. L., and Mueller, L. (1988) Toward complete [1]H NMR spectra in proteins. *J. Magn. Reson. 77*, 166–169.
25. Jeener, J., Meier, B. H., Bachmann, P., and Ernst, R. R. (1979) Investigation of exchange processes by two-dimensional NMR spectroscopy. *J. Chem. Phys. 71*, 4546–4553.
26. Kumar, A., Ernst, R. R., and Wuthrich, K. (1980) A two-dimensional nuclear Overhauser enhancement (2D NOE) experiment for the elucidation of complete proton-proton cross-relaxation networks in biological macromolecules. *Biochem. Biophys. Res. Commun. 95*, 1–6.
27. Piotto, M., Saudek, V., and Sklenar, V. (1992) Gradient-tailored excitation for single-quantum NMR spectroscopy of aqueous solutions. *J. Biomol. NMR 2*, 661–665.
28. Bearden, D. W., Macura, S., and Brown, L. R. (1988) Suppression of cross relaxation in TOCSY experiments on macromolecules. *J. Magn. Reson. 80*, 534–538.
29. Briand, J., and Ernst, R. R. (1991) Computer-optimized homonuclear TOCSY experiments with suppression of cross relaxation. *Chem. Phys. Lett. 185*, 276–285.
30. Griesinger, C., Otting, G., Wuethrich, K., and Ernst, R. R. (1988) Clean TOCSY for proton spin system identification in macromolecules. *J. Am. Chem. Soc. 110*, 7870–7872.
31. Aue, W. P., Bartholdi, E., and Ernst, R. R. (1976) Two-dimensional spectroscopy. Application to nuclear magnetic resonance. *J. Chem. Phys. 64*, 2229–2246.
32. Derome, A. E., and Williamson, M. P. (1990) Rapid-pulsing artifacts in double-quantum-filtered COSY. *J. Magn. Reson. 88*, 177–185.
33. Rance, M., Sorensen, O. W., Bodenhausen, G., Wagner, G., Ernst, R. R., and Wuthrich, K. (1983) Improved spectral resolution in COSY 1H NMR spectra of proteins via double quantum filtering. *Biochem. Biophys. Res. Commun. 117*, 479–485.
34. Bartels, C., Xia, T.-h., Billeter, M., Güntert, P., and Wüthrich, K. (1995) The program XEASY for computer-supported NMR spectral analysis of biological macromolecules. *J. Biomol. NMR 6*, 1–10.
35. Goddard, T. D., and Kneller, D. G. *SPARKY 3*, 3rd ed., University of California, San Francisco, CA.
36. Salgueiro, C. A., Turner, D. L., and Xavier, A. V. (1997) Use of paramagnetic NMR probes for structural analysis in cytochrome c3 from *Desulfovibrio vulgaris*. *Eur. J. Biochem. 244*, 721–734.
37. Turner, D. L., Brennan, L., Meyer, H. E., Lohaus, C., Siethoff, C., Costa, H. S., Gonzalez, B., Santos, H., and Suarez, J. E. (1999) Solution structure of plantaricin C, a novel lantibiotic. *Eur. J. Biochem. 264*, 833–839.
38. Guntert, P., and Wuthrich, K. (1991) Improved efficiency of protein structure calculations from NMR data using the program DIANA with redundant dihedral angle constraints. *J. Biomol. NMR 1*, 447–456.
39. Wareham, R. S., Kilburn, J. D., Rees, N. H., Turner, D. L., Leach, A. R., and Holmes, D. S. (1995) Synthesis and solution conformation of a C2 symmetric macrobicycle. *Tetrahedron Lett. 36*, 3047–3050.
40. Wareham, R. S., Kilburn, J. D., Turner, D. L., Rees, N. H., and Holmes, D. S. (1996) Homeomorphic isomerism in a peptidic macrobicycle. *Angew. Chem. Int. Ed., Engl. 34*, 2660–2662.
41. Turner, D. L., Brennan, L., Chamberlin, S. G., Louro, R. O., and Xavier, A. V. (1998) Determination of solution structures of paramagnetic proteins by NMR. *Eur. Biophys. J. 27*, 367–375.
42. Bertini, I., Donaire, A., Felli, I. C., Rosato, A., and Luchinat, C. (1996) From NOESY cross peaks to structural constraints in a paramagnetic metalloprotein. *Magn. Reson. Chem. 34*, 948–950.
43. Bertini, I., Felli, I. C., Luchinat, C., and Rosato, A. (1996) A complete relaxation matrix refinement of the solution structure of a paramagnetic metalloprotein: reduced HiPIP I from *Ectothiorhodospira halophila*. *Proteins 24*, 158–164.
44. Bertini, I., and Luchinat, C. (1986) NMR of Paramagnetic Molecules in Biological Systems, Benjamin/Cummings Pub. Co., Menlo Park, CA.
45. Boelens, R., Koning, T. M. G., and Kaptein, R. (1988) Determination of biomolecular structures from proton-proton NOE's using a relaxation matrix approach. *J. Mol. Struct. 173*, 299–311.
46. Boelens, R., Koning, T. M. G., van der Marel, G. A., van Boom, J. H., and Kaptein, R. (1989) Iterative procedure for structure determination from proton-proton NOEs using a full relaxation matrix approach. Application to a DNA octamer. *J. Magn. Reson. 82*, 290–308.
47. Turner, D. L. (1993) Evaluation of 13C and 1H Fermi contact shifts in horse cytochrome c. The origin of the anti-Curie effect. *Eur. J. Biochem. 211*, 563–568.
48. Paixao, V. B., Salgueiro, C. A., Brennan, L., Reid, G. A., Chapman, S. K., and Turner, D. L. (2008) The solution structure of a tetraheme cytochrome from *Shewanella frigidimarina* reveals a novel family structural motif. *Biochemistry 47*, 11973–11980.
49. Pettersen, E. F., Goddard, T. D., Huang, C. C., Couch, G. S., Greenblatt, D. M., Meng, E. C., and Ferrin, T. E. (2004) CSF chimera: a visualization system for exploratory research and analysis. *J. Comput. Chem. 25*, 1605–1612.
50. Koradi, R., Billeter, M., and Wüthrich, K. (1996) MOLMOL: a program for display and analysis of macromolecular structures. *J Mol Graphics 14*, 51–55.
51. Vriend, G. (1990) WHAT IF: A molecular modeling and drug design program. *J. Mol. Graphics 8*, 52–56.
52. Hutchinson, E. G., and Thornton, J. M. (1996) PROMOTIF: a program to identify and analyze structural motifs in proteins. *Protein Sci. 5*, 212–220.
53. Williamson, M. P., and Asakura, T. (1993) Empirical comparisons of models for chemical-shift calculation in proteins. *J. Magn. Reson., Ser. B 101*, 63–71.
54. Wüthrich, K. (1986) NMR of Proteins and Nucleic Acids, pp 30−31, 130−161, John Wiley and Sons, New York.
55. Guntert, P., Braun, W., and Wuthrich, K. (1991) Efficient computation of three-dimensional protein structures in solution from nuclear magnetic resonance data using the program DIANA and the supporting programs CALIBA, HABAS and GLOMSA. *J. Mol. Biol. 217*, 517–530.
56. Ramachandran, G. N., Ramakrishnan, C., and Sasisekharan, V. (1963) Stereochemistry of polypeptide chain configurations. *J. Mol. Biol. 7*, 95–99.
57. Barry, C. D., North, A. C., Glasel, J. A., Williams, R. J., and Xavier, A. V. (1971) Quantitative determination of mononucleotide conformations in solution using lanthanide ion shift and broadenine NMR probes. *Nature 232*, 236–245.
58. Barry, C. D., Martin, D. R., Williams, R. J., and Xavier, A. V. (1974) Quantitative determination of the conformation of cyclic 3′,5′-adenosine monophosphate in solution using lanthanide ions as nuclear magnetic resonance probes. *J. Mol. Biol. 84*, 491–502.
59. Gochin, M., and Roder, H. (1995) Protein structure refinement based on paramagnetic NMR shifts: applications to wild-type and mutant forms of cytochrome c. *Protein Sci. 4*, 296–305.
60. Turner, D. L., Brennan, L., Messias, A. C., Teodoro, M. L., and Xavier, A. V. (2000) Correlation of empirical magnetic susceptibility tensors and structure in low-spin heme proteins. *Eur. Biophys. J. 29*, 104–112.
61. Turner, D. L. (2000) Obtaining ligand geometries from paramagnetic shifts in low-spin heme proteins. *J. Biol. Inorg. Chem. 5*, 328–332.
62. Baptista, A. M., Martel, P. J., and Soares, C. M. (1999) Simulation of electron-proton coupling with a Monte Carlo method: application to cytochrome c3 using continuum electrostatics. *Biophys. J. 76*, 2978–2998.